Magnetic excitations in $Tb_2Sn_2O_7$ and $Tb_2Ti_2O_7$ as measured by inelastic neutron scattering

I. Mirebeau,[1] P. Bonville,[2] and M. Hennion[1]
[1]*Laboratoire Léon Brillouin, CEA-CNRS, CE-Saclay, 91191 Gif-sur-Yvette, France*
[2]*DSM/Service de Physique de l'Etat Condensé, CEA-CNRS, CE-Saclay, 91191 Gif-Sur-Yvette, France*
(Received 29 June 2007; revised manuscript received 13 September 2007; published 27 November 2007)

We have measured the magnetic excitations by inelastic neutron scattering in the paramagnetic phase down to 1.6 K, in $Tb_2Ti_2O_7$, which remains spin liquid down to 0.05 K, and in $Tb_2Sn_2O_7$, which shows an ordered spin ice state below 1.3 K. The temperature dependence of the crystal field excitations, measured in the energy range 0–10 THz, shows striking differences between the two compounds. The neutron data were reasonably reproduced by a set of crystal field parameters, showing that while the two compounds have similar values of the gap between the first two crystal field doublets, the associated wave functions are exchanged. This difference comes from a change in sign of the crystal field parameter B_6^0. The neutron data also suggest that an excitation at very low energy (about 0.03 THz) is present in both compounds. Using these sets of crystal field parameters, the high field magnetization and low field susceptibility data can be correctly reproduced by taking the exchange interaction into account in the molecular field approximation. The values obtained for the exchange integral are discussed.

DOI: 10.1103/PhysRevB.76.184436 PACS number(s): 71.30.+h, 71.27.+a, 75.25.+z

I. INTRODUCTION

Geometrically frustrated pyrochlore magnets are now intensively studied, both theoretically and experimentally. The geometrical frustration of the lattice of corner sharing tetrahedra inhibits the formation of a collinear long range order, leading to a wide variety of magnetic behaviors, such as spin liquids, spin ices, chemically ordered spin glasses, or uncollinear long range orders.[1]

Among them, the rare earth pyrochlore $Tb_2Ti_2O_7$ is one of the most studied. $Tb_2Ti_2O_7$ has been called a spin liquid due to the presence of first neighbor antiferromagnetic (AF) correlations between fluctuating spins. The slowing down of the spin fluctuations was studied by muon spin rotation (μSR) and inelastic neutron scattering.[2–4] $Tb_2Ti_2O_7$ shows an absence of long range order (LRO) and the persistence of spin dynamics down to extremely low temperatures (50 mK), despite large antiferromagnetic interactions with a Curie-Weiss temperature θ_{CW} from -19 to -15 K.

The absence of LRO in $Tb_2Ti_2O_7$ has for long remained a mystery in theory.[5,6] Monte Carlo simulations with classical Ising spins interacting via AF exchange interactions and dipolar coupling predict for $Tb_2Ti_2O_7$ the onset of AF order at about 1.2 K.[7] Under pressure and stress, long range antiferromagnetic order is restored,[8] with a Néel temperature which may be tuned by the orientation of the stress with respect to the crystal axes.[9] AF long range order with spin wave dispersion is induced under a high magnetic field,[10] likely due to magnetostriction effects. Spin-glass-like irreversibilities[11,12] were observed below 1 K and a short range antiferromagnetic structure, ordered within a few cubic cells, was observed at 50 mK,[13] both features being likely induced by internal stress.

The key parameters in $Tb_2Ti_2O_7$, believed to be responsible for its surprising behavior, are (i) an AF near neighbor exchange interaction with a value close to the ferromagnetic (F) near neighbor dipolar interaction, yielding a small effective AF exchange in the classical approximation and the proximity of the system near a Néel to spin ice phase boundary, and (ii) the existence of low lying crystal field levels of the Tb^{3+} ion. The first crystal field levels consist of two doublets separated by a small energy gap δ of about 18 K or 0.375 THz.[3,14] This feature contrasts with the classical spin ices $Ho_2Ti_2O_7$ and $Dy_2Ti_2O_7$ where the first excited crystal field level is situated well above the ground state.[15–17]

In the parent compound $Tb_2Sn_2O_7$, neutron diffraction experiments[18] showed a transition toward long range magnetic order. In the "ordered spin ice" structure observed in $Tb_2Sn_2O_7$, magnetic moments in a given tetrahedron orient close to the $\langle 111 \rangle$ anisotropy axes, in the "two in-two out" configuration of the local spin ice structure. However, in contrast to the classical spin ices which do not order at large scale, here the four tetrahedra in the cubic unit cell are identical, yielding long range magnetic order with a correlation length up to 200 Å. The onset of Bragg peaks is observed below 1.3 K, with an upturn of the ordered moment at $T_N \sim 0.87$ K, associated with a peak in the specific heat. The basic features of the ordered spin ice structure could be explained within the phenomenological model of Champion *et al.*,[19] which assumes a *ferromagnetic* first neighbor exchange interaction combined with a finite anisotropy.

The first reason for the different behaviors in the two compounds could be the lattice expansion induced by replacing Ti by Sn. The lattice constant a of the cubic unit cell expands from 10.335 Å (Ti) to 10.426 Å (Sn). The lattice expansion should reduce the weight of the AF exchange term with respect to that of the F dipolar first neighbor term, yielding an effective ferromagnetic exchange in $Tb_2Sn_2O_7$ and a crossing of the spin ice boundary.[13] Magnetic fluctuations still play a prominent role in the ordered spin ice state of $Tb_2Sn_2O_7$, inducing a strong reduction of the ordered moment as measured using the hyperfine Schottky anomaly of the specific heat.[18] These fluctuations were recently probed by μSR experiments.[20,21] How they microscopically coexist with the ordered state is still an open question.

The crystal field (CF) scheme of the Tb^{3+} ion also plays a key role in determining the magnetic ground state of the two

compounds. The specific CF scheme of the Tb^{3+} ion has been studied in $Tb_2Ti_2O_7$ by several authors.[14,22–24] It is responsible for its giant magnetostriction,[22,24] 1 order of magnitude greater than for the other rare earth compounds of the same family. It could also be a key ingredient to explain why $Tb_2Ti_2O_7$ does not order, whereas $Tb_2Sn_2O_7$ undergoes LRO.

$Tb_2Ti_2O_7$ was recently considered[25] as a novel quantum variant of the classical Ising spin ice with "dynamically induced frustration," implying that quantum fluctuations are responsible for the lack of LRO. Such fluctuations would arise from virtual transitions to excited single-ion crystal field levels and many body interactions.[25] On the other hand, in $Tb_2Sn_2O_7$ the onset of long range order, not observed in classical spin ices, has been attributed to the fact that the crystal field anisotropy is smaller than in spin ices, yielding a behavior intermediate between spin ice and Heisenberg ferromagnet.[19] In other words, in $Tb_2Sn_2O_7$, the spin ice orders because it would be a "soft" spin ice. In this context, a precise determination of the crystal field excitations in $Tb_2Sn_2O_7$ and $Tb_2Ti_2O_7$ is of crucial importance. The most precise determination is given by inelastic neutron scattering, which provides information on both energy and intensities of the CF transitions, without perturbing the system by a magnetic field.

In this work, we have performed inelastic neutron scattering measurements in the two compounds, down to 1.6 K, in the paramagnetic phase. The use of both cold and thermal neutrons allows us to measure the low energy excitations with great accuracy and to cover a large energy range (up to 10 THz). We can therefore improve the measurements previously performed[14] in $Tb_2Ti_2O_7$ and obtain high quality data in $Tb_2Sn_2O_7$, where the CF excitations have not been measured up to now. We also present isothermal magnetization measurements between 1.7 and 20 K with a field up to 14 T and magnetic susceptibility data up to 250 K, measured with a field of 0.005 T. Comparing the data in the two compounds measured in the same conditions allows us to probe qualitative differences in their CF level scheme.

These differences can be quantitatively interpreted by diagonalizing the CF Hamiltonian and searching for a set of CF parameters that reasonably reproduces the energies and intensities of the transitions. Confidence in the derived set of parameters is enhanced if the data are correctly reproduced in the large temperature range (1.4–40 K) of our experiments. We find that while the two compounds have similar values of the gap δ between the first two doublets, the associated wave functions are exchanged in $Tb_2Ti_2O_7$ and $Tb_2Sn_2O_7$. This explains why some particular inelastic transitions, not observed in $Tb_2Ti_2O_7$, are present in $Tb_2Sn_2O_7$. The determination of the CF parameters also allows one to calculate the high field magnetization in the paramagnetic range, in good agreement with experiments performed up to 14 T. Besides the CF excitations, our neutron measurements also suggest the presence of another excitation at very low energy in both compounds, whose origin is discussed.

In Sec. II, we give details about samples and experiments. Then, we describe the inelastic neutron scattering results (Sec. III) and the CF calculation (Sec. IV). The magnetic measurements are shown in Sec. V, and the anisotropic magnetic behavior of the Tb^{3+} ion is studied in Sec. VI. Section VII contains an overall discussion of the results.

II. EXPERIMENTAL DETAILS

Powder samples of $Tb_2Ti_2O_7$ and $Tb_2Sn_2O_7$ of about 15 g, synthesized in the same way as for previous experiments,[8,18] were characterized by powder neutron and x-ray diffraction. They were put in aluminum sample holders inserted in a cryostat, reaching a minimal temperature of about 1.6 K. The inelastic neutron scattering experiments were performed in the Laboratoire Léon Brillouin. We used triple axis spectrometers on a cold neutron source (spectrometers 4F1 and 4F2) and on a thermal neutron source (spectrometers 1 T and 2 T). Measurements were performed with constant values of the outcoming wave vector $\mathbf{k}_f$. Several sets of measurements were performed with different k_f values, namely, $k_f=1.48$ and 1.64 $Å^{-1}$ (cold neutron source) and $k_f=1.97$ and 2.662 $Å^{-1}$ (thermal neutron source, filtered by a pyrolytic graphite). This procedure allowed us to cover a broad energy range (0–10 THz), keeping a good resolution at low energies. The energy resolution at full width half maximum was about 0.04, 0.06, 0.1, and 0.26 THz for $k_f=1.48$, 1.64, 1.97, and 2.662 $Å^{-1}$, respectively. We systematically performed experiments on both Ti and Sn samples in the same experimental conditions.

Magnetic measurements were performed in the Service de Physique de l'Etat Condensé. The high field magnetization data were obtained in a Cryogenic vibrating sample magnetometer operating between 1.7 and 300 K, with a maximum field of 14 T, and the susceptibility data in a Cryogenic superconducting quantum interference device magnetometer.

III. INELASTIC NEUTRON SCATTERING RESULTS

We consider successively the low energy range (up to 0.8 THz), the medium energy range (up to 4 THz), and the high energy range (up to 10 THz). In each case, the energy resolution was chosen to measure the crystal field excitations in the best conditions.

A. Low energy excitations

In the low energy range (up to 0.8 THz), constant Q scans were measured on triple axis spectrometers installed on the cold source with $k_f=1.48$ $Å^{-1}$ in the Q range (0–2.2 $Å^{-1}$) at 1.6, 20, and 40 K. They allowed measurement of the neutron intensity in the region of the elastic peak together with the first crystal field excitation, situated around 0.3–0.4 THz in both samples. Typical scans at 1.6 K are shown for both compounds in Fig. 1. The neutron intensity was fitted with the sum of three contributions: an elastic one and a quasielastic or a weakly inelastic one to account for the central region, and an inelastic contribution for the first crystal field excitation.

The Q and T dependences of the energy, energy width, and integrated intensity of this excitation, shown in Fig. 2, are quite similar for the two samples. As already noticed[3,14] for $Tb_2Ti_2O_7$, this excitation shows an energy dispersion at low temperature (1.6 and 1.9 K for Sn and Ti samples, re-

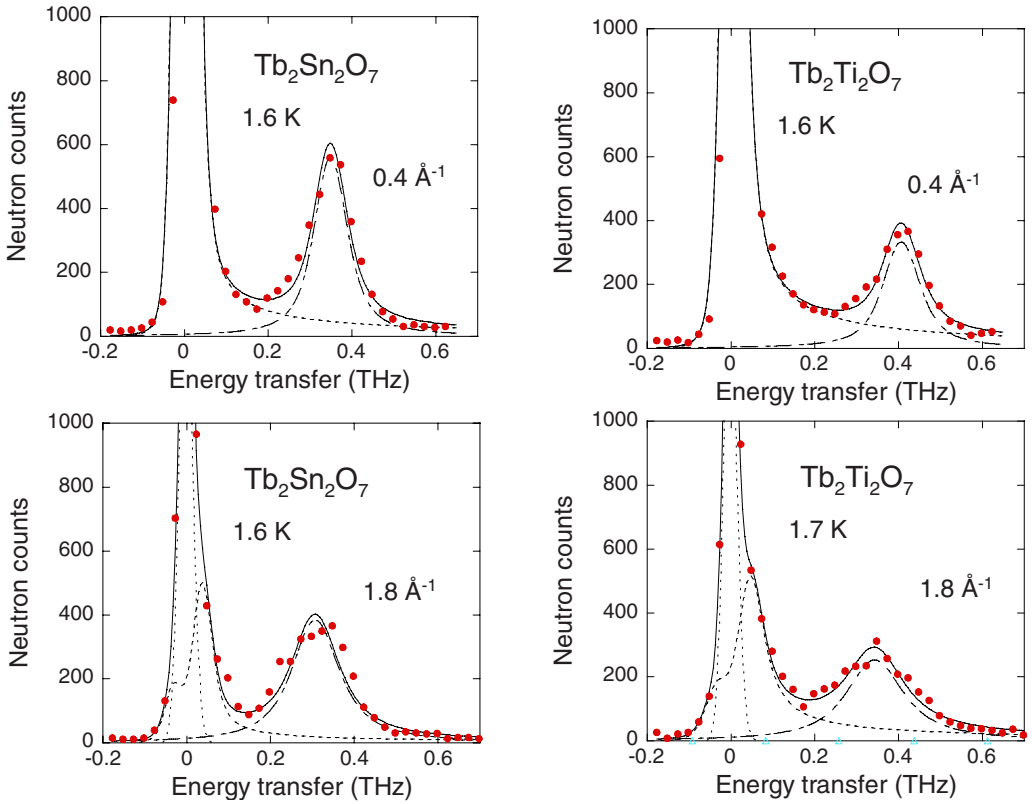

FIG. 1. (Color online) Constant Q scans showing the low energy and first crystal field excitation around 0.3 THz, measured in $Tb_2Sn_2O_7$ and $Tb_2Ti_2O_7$ for Q values of 0.4 and 1.8 Å^{-1} at 1.6 K, with k_f=1.48 Å^{-1}. The solid line is the total fitted curve and the dotted, dashed, and dashed-dotted lines are the fitted contributions from the elastic peak, the low energy mode, and the first crystal field excitation, respectively. For Q=0.4 Å^{-1}, the elastic contribution is not separated from the weakly inelastic one (low energy mode), of much higher intensity.

spectively), with an energy minimum at about 1.1 Å^{-1}. The dispersion disappears when heating at about 50 K. The integrated intensity shows a clear maximum at the same Q value, characteristics of the first neighbor distance, as also seen by the liquidlike shape of the structure factor measured in diffraction experiment.[2] The inverse variations of the dispersion and structure factor are reminiscent of the excitation spectrum of liquid He. In $Tb_2Ti_2O_7$, the dispersion of the first CF level was well studied by single crystal experiments[3,10] and could be reproduced by calculations in the random-phase approximation, taking CF excitations, first neighbor exchange, and dipolar interactions into account.[5] The Q dependence of the energy width is about featureless.

The central region is well fitted by a quasielastic contribution, except at low temperature (1.6 K) where a weakly inelastic contribution, with a typical energy of about 0.03–0.04 THz, yields a better agreement to the data. This excitation is better seen at high Q values, whereas at low Q values, its intensity becomes much stronger than that of the elastic peak, which cannot be easily separated from it (Fig. 1). The energy and energy width of this excitation (Fig. 3) were determined with rather good confidence in the Q range 0.4–2.2 Å^{-1} by constraining the position of the elastic peak to zero energy. The origin of this excitation, not seen before, may not simply arise from CF excitations and it will be considered separately. By extrapolating its energy at Q=0, one finds a gap of about 0.028(3) and 0.034(3) THz in $Tb_2Sn_2O_7$ and $Tb_2Ti_2O_7$, respectively. Figure 3 also shows that in $Tb_2Sn_2O_7$, this excitation is better defined than in $Tb_2Ti_2O_7$, showing a smaller energy width and a slight dispersion. The origin of this excitation will be briefly discussed in Sec. VII.

B. Medium energy range

The medium energy range (up to 4 THz) was studied on triple axis spectrometers installed on the cold source, with k_f=1.64 Å^{-1}. Here, one observes CF excitations around 2.5 and 3.6 THz. As previously seen in $Tb_2Ti_2O_7$, these excitations show a very small dispersion, of about 3%–5%, much less pronounced than for the first excitation.[5]

They were studied versus temperature up to about 40 K, for a Q value of 2 Å^{-1}, and showed very different behaviors for $Tb_2Sn_2O_7$ (Fig. 4) and $Tb_2Ti_2O_7$ (Fig. 5). In $Tb_2Sn_2O_7$, two excitations are observed at 2.3 and 2.6 THz, whose intensities strongly vary with temperature (Fig. 6). The intensity of the excitation at 2.6 THz decreases when heating, whereas those of the excitations at 2.3 and 3.6 THz increase. As shown below, this is explained by a change in the Boltzmann populations of the two lowest crystal field levels. In contrast, in $Tb_2Ti_2O_7$, a unique excitation is observed at 2.5 THz, whose intensity decreases when heating. Here, the intensity of the excitation at 3.6 THz almost does not change with temperature, up to 40 K (Fig. 6).

C. High energy range

In the high energy range (up to 10 THz), measurements were performed on triple axis spectrometers installed on the

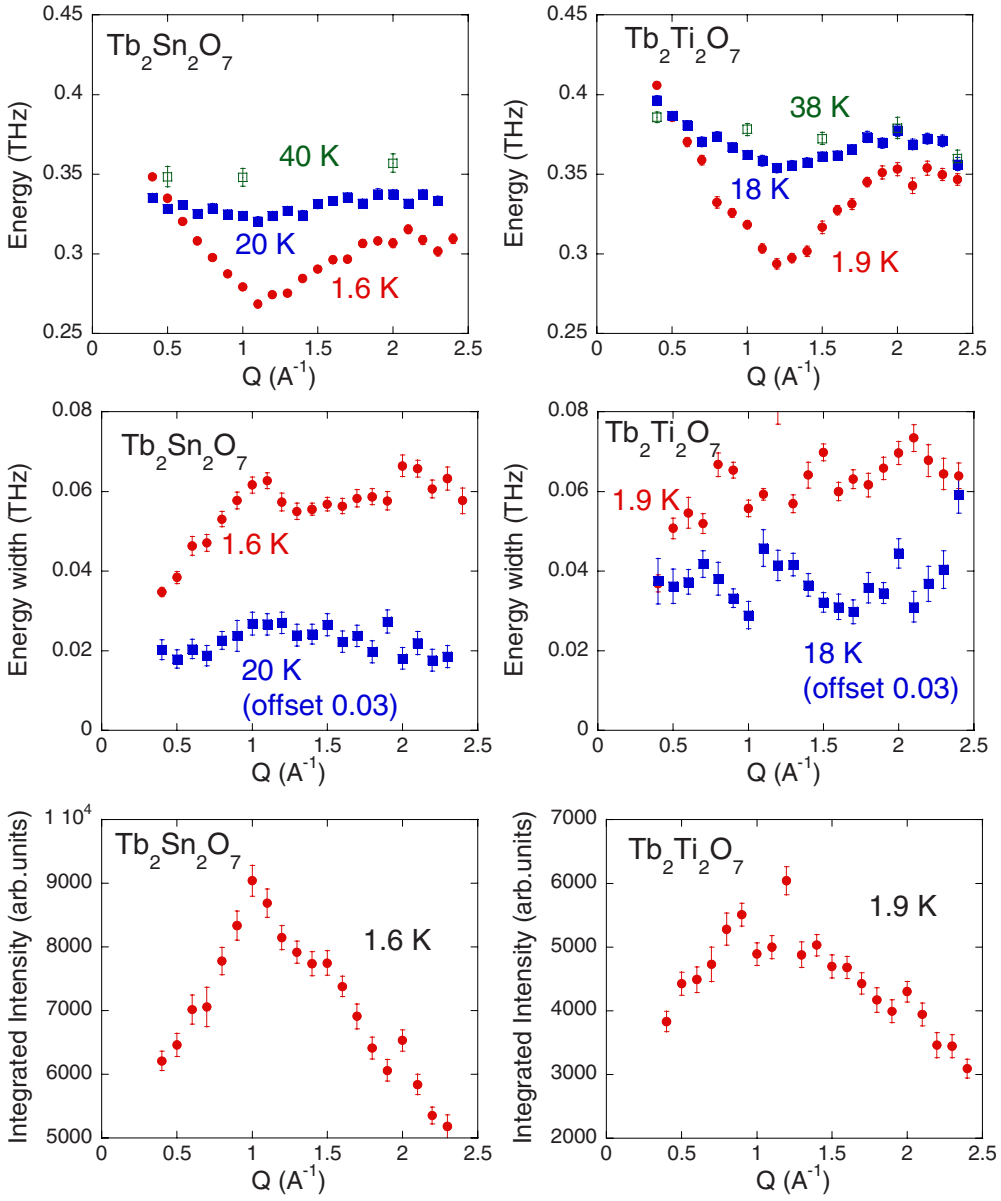

FIG. 2. (Color online) First crystal field excitation in $Tb_2Sn_2O_7$ (left) and $Tb_2Ti_2O_7$ (right): Q dependence of the energy (top), energy width (middle), and integrated intensity (bottom). Filled dots, T=1.6 or 1.9 K; filled squares, T=20 or 18 K; open squares, T=40 or 38 K.

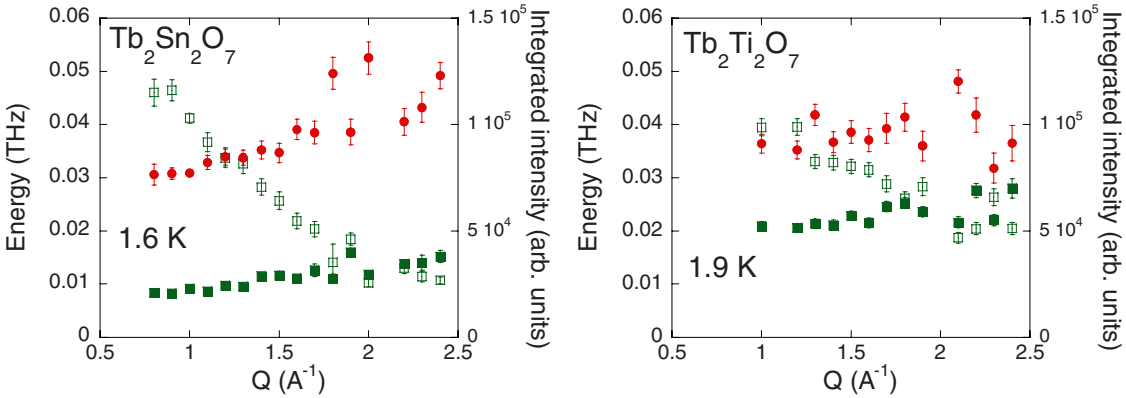

FIG. 3. (Color online) Low energy mode in $Tb_2Sn_2O_7$ (left) and $Tb_2Ti_2O_7$ (right) measured with k_f=1.48 Å^{-1}: Q dependence of the energy (filled dots), energy width (filled squares), and integrated intensity (open squares).

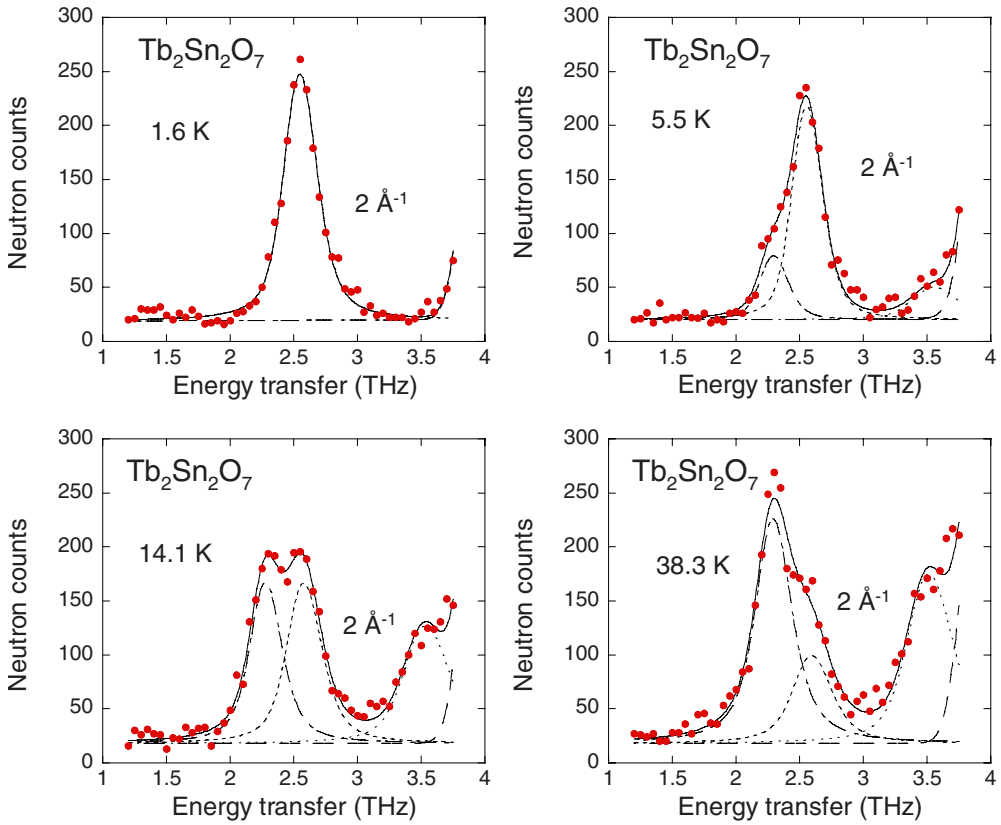

FIG. 4. (Color online) $Tb_2Sn_2O_7$: constant Q scans, showing the crystal field excitations around 2.5 and 3.6 THz for several temperatures, measured with k_f=1.64 Å^{-1}. The solid line is the total fitted curve, the dashed line is the background contribution, and the dotted and dashed-dotted lines are the fitted contributions from the individual excitations. The excitation at 3.6 THz is on the slope of a background peak.

thermal source with k_f=2.662 Å^{-1}, for Q=2, 3, and 4 Å^{-1}. They allowed another excitation to be observed at 4.2(1) and 4.0(1) THz for $Tb_2Sn_2O_7$ and $Tb_2Ti_2O_7$, respectively. This excitation could not be seen on the spectrometers using cold neutrons due to a high background contribution. Moreover, scans for Q=3 and 4 Å^{-1} showed one extra crystal field excitation at 7.8 THz in $Tb_2Sn_2O_7$, which is very small in $Tb_2Ti_2O_7$ (Fig. 7). Finally, energy scans measured for Q =2 Å^{-1} with an intermediate k_f value of 1.97 Å^{-1} allowed us to measure most of the crystal field excitations in the same scan, and therefore to determine their relative intensities with a good accuracy.

D. Data treatment and reconstructed spectra

The neutron cross section is expressed versus the neutron intensity by the expression

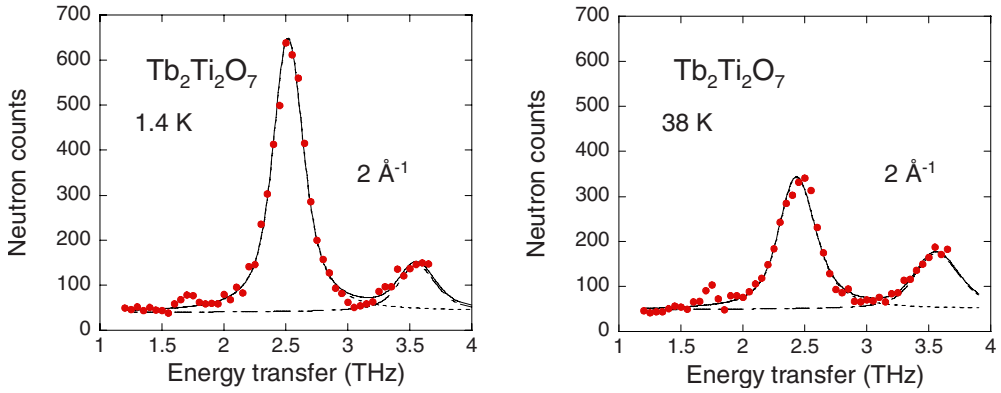

FIG. 5. (Color online) $Tb_2Ti_2O_7$: crystal field excitations around 2.5 and 3.5 THz for Q=2 Å^{-1}, at 1.4 and 38 K, measured with k_f =1.64 Å^{-1}. The solid line is the total fitted curve. The dashed line is the background contribution. The dotted and dashed-dotted lines are the fitted contributions from the individual excitations.

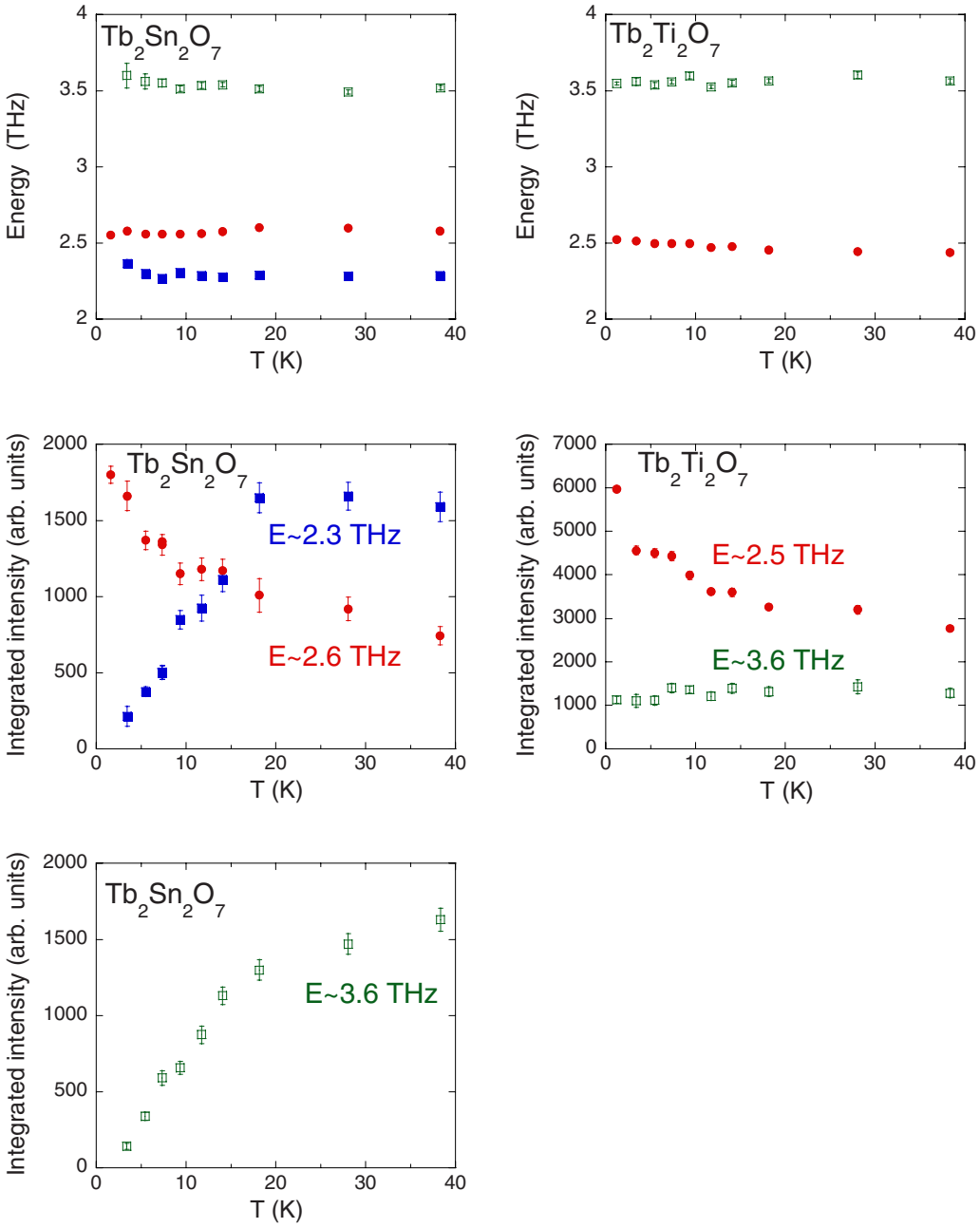

FIG. 6. (Color online) Crystal field excitations around 2.5 and 3.6 THz in $Tb_2Sn_2O_7$ (left) and $Tb_2Ti_2O_7$ (right): temperature dependence of the energy (top), and integrated intensity (middle and bottom) for $Q=2$ Å^{-1}, $k_f=1.64$ Å^{-1}. Filled squares, filled dots, and open squares correspond to the excitations around 2.3, 2.6, and 3.6 THz, respectively.

$$\frac{d^2\sigma}{d\Omega d\omega} = \frac{k_f}{k_i} CI(Q,\omega), \tag{1}$$

where k_i and k_f are the moduli of the incident and outcoming wave vectors, respectively, and C is a constant.

The neutron intensity at the wave vector Q_0 and energy transfer ω_0 is expressed as

$$I(Q_0,\omega_0) = \sum_{i,j} N_{ij}(Q_0) \int R(\omega-\omega_0) S_{ij}(\omega) d\omega, \tag{2}$$

where $R(\omega-\omega_0)$ is the resolution function centered at ω_0. Its Q dependence is omitted in Eq. (2) for simplicity. The integration is performed over all energy transfers ω. The sum is performed over the transitions from the CF state $|i\rangle$ of energy E_i to the state $|j\rangle$ of energy E_j.

$S_{ij}(\omega)$ is the normalized spectral function of the excitation from state $|i\rangle$ to state $|j\rangle$ taken Lorentzian shaped:

$$S_{ij}(\omega) = \frac{1}{\pi} \frac{\Gamma_{ij}}{\Gamma_{ij}^2 + (\omega-\omega_{ij})^2}, \tag{3}$$

where ω_{ij} and Γ_{ij} correspond to the energy and intrinsic energy half-width at half maximum of the excitation, respectively. For a given transition from the CF state $|i\rangle$ of energy E_i to the state $|j\rangle$ of energy E_j (with $\hbar\omega_{ij}=E_i-E_j$), the nor-

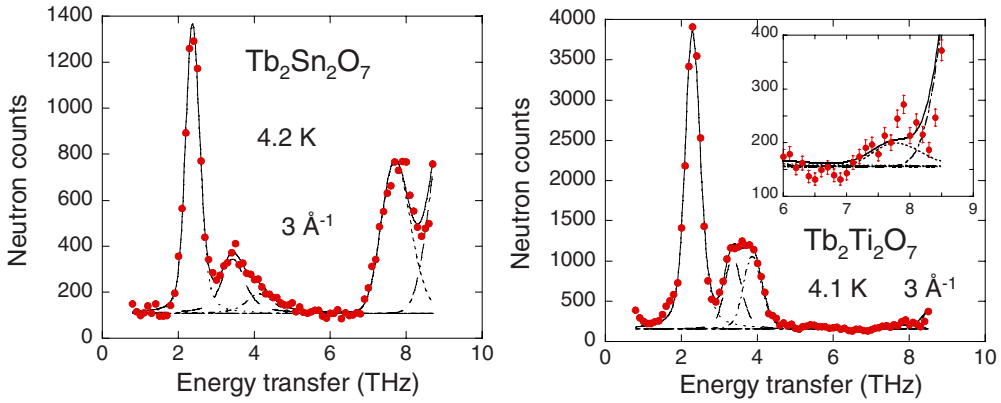

FIG. 7. (Color online) Crystal field excitations in the high energy range in $Tb_2Sn_2O_7$ (left) and $Tb_2Ti_2O_7$ (right), measured at 4 K for $Q=3$ Å^{-1}, with $k_f=2.662$ Å^{-1}. Inset: Same spectrum with an enlarged scale around 8 THz. The excitation at 7.8 THz is on the slope of a background peak. The solid line is the total fitted curve. The dashed line is the background contribution. The dotted and dashed-dotted lines are the fitted contributions from the individual excitations.

malized intensity of the transition N_{ij} is related to the transition probability of the excitation by the expression

$$N_{ij} = Ap_iF(Q)^2|\langle j|\mathbf{m}_\perp|i\rangle|^2, \tag{4}$$

where $F(Q)$ is the magnetic form factor of Tb^{3+}, p_i is the occupancy (Boltzmann factor) of the level i, $\mathbf{m}_\perp$ is the magnetic component of the magnetic moment operator perpendicular to the scattering vector $\mathbf{Q}$ and A is a constant.

The set of parameters (N_{ij}, ω_{ij}, Γ_{ij}) was fitted for each excitation, allowing us to build the "reconstructed" energy spectra shown in Fig. 8 for $Tb_2Ti_2O_7$ and Fig. 10 for $Tb_2Sn_2O_7$. Spectra are shown for $k_f=1.64$ (cold neutrons) and 1.97 Å^{-1} (thermal neutrons). The reconstructed spectra correspond to $Q=2$ Å^{-1}, a value which situates in a Q range where the dispersion of the low energy excitation is negligible. The intensity of the high energy excitation (7.8 THz), which could be seen only for $Q=3$ and 4 Å^{-1}, was calibrated for $Q=2$ Å^{-1} using other excitations at lower energies. The Q dependence of the excitations was therefore neglected in the further analysis. The reconstructed spectra were compared with the calculated ones, allowing an easy check of the validity of the calculation.

IV. CRYSTAL FIELD CALCULATION

In the following calculation, the small Q and T dependences of the energies of the excitations are neglected. The single-ion crystal field interaction for trigonal symmetry writes, according to Stevens,[26] Hutchings,[29] and Abragam and Bleaney,[30]

$$\mathcal{H}_{\mathrm{CF}} = \alpha_J D_2^0 O_2^0 + \beta_J (D_4^0 O_4^0 + D_4^3 O_4^3) + \gamma_J (D_6^0 O_6^0 + D_6^3 O_6^3 + D_6^6 O_6^6), \tag{5}$$

where the D_n^m are coefficients with $n<2l$ ($l=3$ for rare earths) and $|m|\leqslant n$. The operator equivalents O_n^m are tabulated in Ref. 30, and the coefficients are $\alpha_J=-1/99$, $\beta_J=2/16335$, and $\gamma_J=-1/891\,891$ for Tb^{3+}. Another formulation of this interaction is in terms of spherical harmonics:[29]

$$\mathcal{H}'_{\mathrm{CF}} = \sum_{n,m} B_n^m \sqrt{\frac{4\pi}{2n+1}} Y_n^m, \tag{6}$$

the relationship between the two types of coefficients being $D_n^m=\lambda_n^m B_n^m$, where the λ_n^m are given for Tb^{3+} in Table I. As the latter convention is used in the recent literature about crystal field in rare earth pyrochlores,[14,31] we will use it here also. However, we will only consider the ground spin-orbit multiplet of the Tb^{3+} ion, with $J=6$, whereas the calculations in Refs. 14 and 31 include the excited spin-orbit multiplets. Therefore, a precise comparison of the CEF parameters derived here with those of the literature can only be approximate.

The reconstructed spectra in $Tb_2Ti_2O_7$, as shown in Fig. 8, are similar to the spectra obtained in Ref. 14 in the energy range up to 5 THz. Our data taken up to 10 THz show only a very small extra line around 8 THz. According to the analysis made in Ref. 14, the lowest CF levels are arranged as shown in Fig. 9, with two close ground doublets and two upper singlets. The lowest energy transition, labeled 1 in Fig. 9, corresponds to the first inelastic peak at $\delta=0.32(3)$ THz in Fig. 8 (top). Then, at finite temperature, all other inelastic excitations should appear as "doublets," corresponding, respectively, to transitions labeled {2,3} and {4,5} in Fig. 9, separated by an energy δ. However, only two inelastic peaks appear in Fig. 8 (bottom), instead of four. This means that there occur accidental line extinctions, which must be explained by the particular CF wave functions in the material. This is clear when looking at the reconstructed spectra in $Tb_2Sn_2O_7$ (Fig. 10). The spectra with thermal neutrons show

TABLE I. Values of the λ_n^m parameters for Tb^{3+}.

λ_2^0	λ_4^0	λ_4^3	λ_6^0	λ_6^3	λ_6^6
$1/2$	$1/8$	$-\sqrt{35}/2$	$1/16$	$-\sqrt{105}/8$	$\sqrt{231}/16$

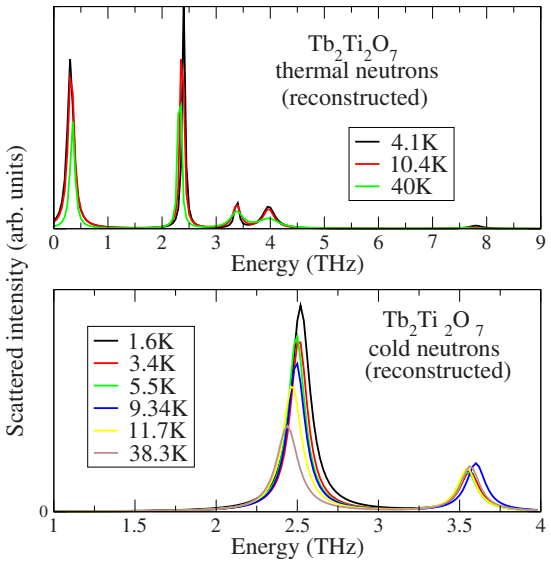

FIG. 8. (Color online) $Tb_2Ti_2O_7$: experimental reconstructed inelastic spectra from the triple axis spectrometers on thermal source (top), for temperatures between 4 and 40 K, and on cold source (bottom), for temperatures between 1.6 and 38 K. The elastic and quasielastic lines are not presented.

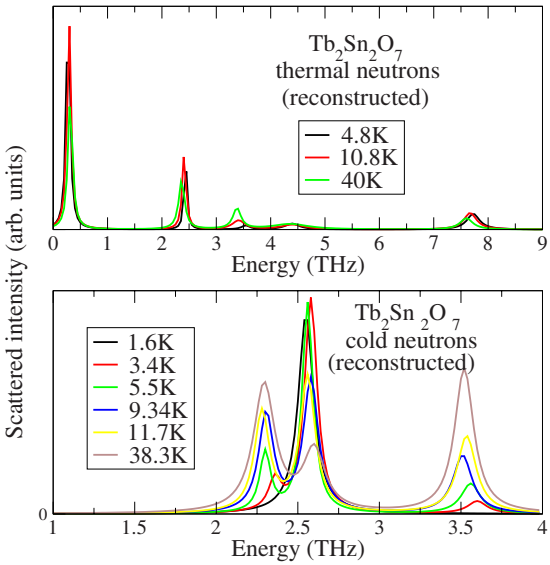

FIG. 10. (Color online) $Tb_2Sn_2O_7$: experimental reconstructed inelastic spectra from the triple axis spectrometers on thermal source (top), for temperatures between 4 and 40 K, and on cold source (bottom), for temperatures between 1.6 and 38 K. The elastic and quasielastic lines are not presented.

lines with energies similar to those in $Tb_2Ti_2O_7$, with, however, a second inelastic line at an energy $\simeq$2.4 THz much less intense relative to the first one. The better resolved spectra with cold neutrons show a picture quite different from that in $Tb_2Ti_2O_7$, with a resolved doublet line around 2.4 THz and a stronger, temperature dependent, line around 3.5 THz. All these features should be explained by finding appropriate CF parameters for both compounds.

We started from the set of B_n^m parameters given for $Tb_2Ti_2O_7$ in Ref. 14, which we refined in order to find a set adapted to our calculation (without account of the excited spin-orbit multiplets) that would reproduce the observed inelastic features in this compound in the whole energy range. We found that the following set reproduces correctly the experimental data (with an uncertainty of 10% on the parameters values):

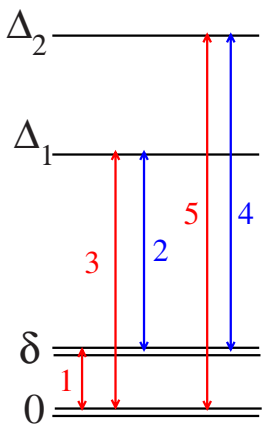

FIG. 9. (Color online) Energy scheme of the four lowest crystal field levels of the Tb^{3+} ion in the Ti and Sn pyrochlore compounds (not to scale).

$$B_2^0 = 491\ \text{cm}^{-1}, \quad B_4^0 = 2345\ \text{cm}^{-1}, \quad B_4^3 = -827\ \text{cm}^{-1},$$

$$B_6^0 = 779\ \text{cm}^{-1}, \quad B_6^3 = 483\ \text{cm}^{-1}, \quad B_6^6 = 786\ \text{cm}^{-1}. \quad (7)$$

The corresponding calculated spectra are represented in Fig. 11. Comparison with Fig. 8 shows a good semiquantitative agreement as concerns line positions and intensities, with, however, small discrepancies. The comparison makes it clear that transition 2 is completely absent, the line at 3.6 THz is transition 5, and transition 4, which indeed is not observed,

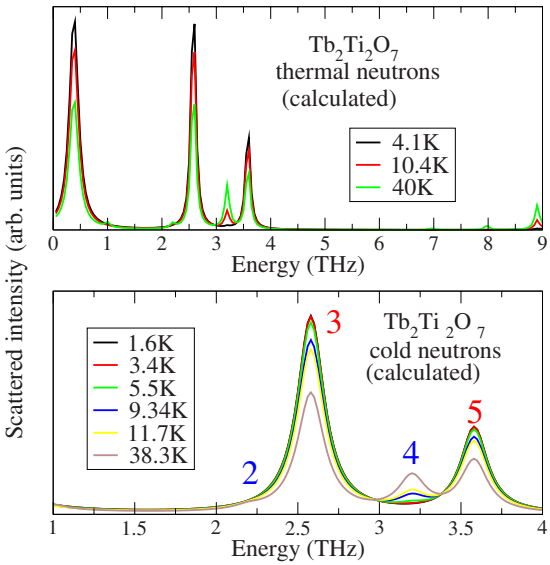

FIG. 11. (Color online) Neutron inelastic spectra in $Tb_2Ti_2O_7$ calculated using the parameter set in Eq. (7) (see text) at the same temperatures as the spectra shown in Fig. 8. The numbers close to the peaks refer to the transition labels in Fig. 9.

TABLE II. Values of the ground state moment, high temperature AF molecular field constant λ, effective exchange integral $\mathcal{J}$, and paramagnetic Curie temperature θ_p^{ex} derived from the high temperature λ value [see Eq. (14)] in $Tb_2Ti_2O_7$ and $Tb_2Sn_2O_7$.

	μ_0 (μ_B)	λ (T/μ_B)	$\mathcal{J}$ (K)	θ_p^{ex}(K)
Ti	5.1	−0.33(1)	−0.083(2)	−7.0(3)
Sn	5.95	−0.30(1)	−0.075(2)	−6.3(3)

appears to be almost absent. The parameter set in Eq. (7) yields δ=0.38 THz, Δ_1=2.58 THz, and Δ_2=3.58 THz, the remaining levels lying at energies higher than 9 THz. The ground wave function is predominantly $|J=6;J_z=\pm 4\rangle$:

$$|\psi_g^{\mathrm{Ti}}\rangle = -0.956|\pm 4\rangle \pm 0.128|\pm 1\rangle - 0.121|\mp 2\rangle \mp 0.226|\mp 5\rangle. \quad (8)$$

This state has an intrinsic moment (i.e., when a small field is applied along a [111] axis) of μ_0=5.1 μ_B. The first excited state has a wave function containing mainly $|J=6;J_z=\pm 5\rangle$:

$$|\psi_1^{\mathrm{Ti}}\rangle = -0.937|\pm 5\rangle \pm 0.241|\pm 2\rangle \mp 0.241|\mp 4\rangle. \quad (9)$$

In both wave functions, the states with coefficients of the order of or less than 0.01 have been omitted; they are close to those obtained in Ref. 14. The value of the ground state moment μ_0=5.1 μ_B (Table II) agrees with a previous determination.[14] The overall CF splitting amounts to about 17 THz or 800 K.

By contrast, in $Tb_2Sn_2O_7$, both transitions 2 and 3 are present and resolved, using cold incident neutrons, and the line at 3.6 THz has a strongly temperature dependent intensity, which suggests that it corresponds to transition 4. So, the wave functions must be substantially different from those in $Tb_2Ti_2O_7$, whereas the level energies are similar. We searched for a set of B_n^m parameters that would meet the requirements of the spectra in $Tb_2Sn_2O_7$, and we found that by changing the sign of the B_6^0 parameter with respect to that in $Tb_2Ti_2O_7$, the main features are reproduced. Refinement of these parameters yields the calculated spectra shown in Fig. 12, obtained with the set (with about 10% uncertainty)

$$B_2^0 = 315\ \mathrm{cm}^{-1},\quad B_4^0 = 1820\ \mathrm{cm}^{-1},\quad B_4^3 = -580\ \mathrm{cm}^{-1},$$
$$B_6^0 = -300\ \mathrm{cm}^{-1},\quad B_6^3 = 228\ \mathrm{cm}^{-1},\quad B_6^6 = 900\ \mathrm{cm}^{-1}. \quad (10)$$

Comparison with Fig. 10 shows that the main features of the inelastic spectra in $Tb_2Sn_2O_7$ are reproduced, in particular, that transition 5 is absent. The parameter set in Eq. (10) yields δ=0.28 THz, Δ_1=2.54 THz, and Δ_2=3.80 THz; three levels (one doublet and two singlets) have energies close to 8 THz, whose transitions are clearly visible in Fig. 10 (top), and the remaining levels lying at energies higher than 10 THz. Contrary to $Tb_2Ti_2O_7$, the ground wave function contains predominantly $|J=6;J_z=\pm 5\rangle$:

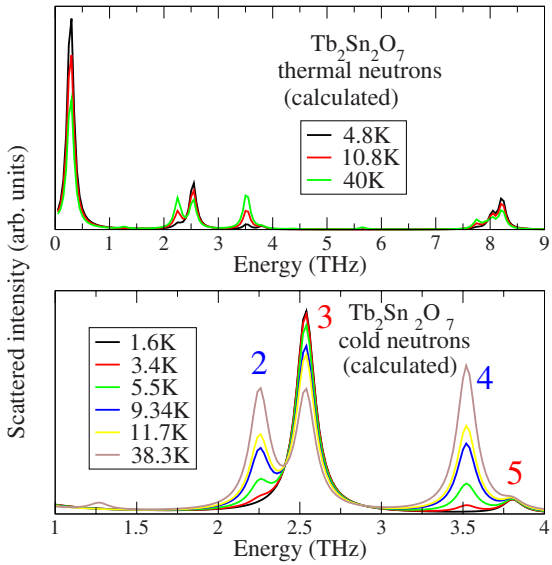

FIG. 12. (Color online) Neutron inelastic spectra in $Tb_2Sn_2O_7$ calculated using the parameter set in Eq. (10) (see text) at the same temperatures as the spectra shown in Fig. 10. The numbers close to the peaks refer to the transition labels in Fig. 9.

$$|\psi_g^{\mathrm{Sn}}\rangle = 0.919|\pm 5\rangle \mp 0.243|\pm 2\rangle + 0.014|\mp 1\rangle \mp 0.309|\mp 5\rangle, \quad (11)$$

which has μ_0=5.95μ_B. This value matches well with the spontaneous moment value of 5.9μ_B measured in the ordered spin ice phase below 0.87 K.[18] The wave function of the first excited state contains mainly $|J=6;J_z=\pm 4\rangle$:

$$|\psi_1^{\mathrm{Sn}}\rangle = 0.935|\pm 4\rangle \mp 0.156|\pm 1\rangle \mp 0.317|\mp 5\rangle. \quad (12)$$

The overall CF splitting is about 12 THz or 580 K. The crystal field level schemes in $Tb_2Ti_2O_7$ and $Tb_2Sn_2O_7$ are therefore very similar as to the energies of the four lowest states, but the wave functions of the ground and first excited state are exchanged. According to our calculation, this is caused by a change in the sign of the B_6^0 CF parameter.

V. MAGNETIC MEASUREMENTS

The isothermal magnetization measurements $m(H)$ were carried out in the temperature range 1.75–20 K. They are shown in Fig. 13 and are very similar in both compounds. In the whole field range up to 14 T, the magnetization increases monotonically and attains 6.3μ_B/Tb ion at the maximum field at 1.75 K. The free ion moment value for Tb^{3+} is $g_J J\mu_B$=9 μ_B (with g_J=3/2 and J=6). Its value is not reached due to CF effects. The low field magnetic susceptibility (χ) was measured in the same conditions for the two compounds, in the range 5–250 K: the nominal applied field was 5 mT, and a residual field of 0.18 mT was measured and taken into account in the calculation of χ. The data are shown as $1/\chi$ in Fig. 14, in the limited temperature range 80–180 K for clarity. Indeed, both experimental data follow effective Curie-Weiss laws very close to each other, where the effective paramagnetic Curie temperature contains a

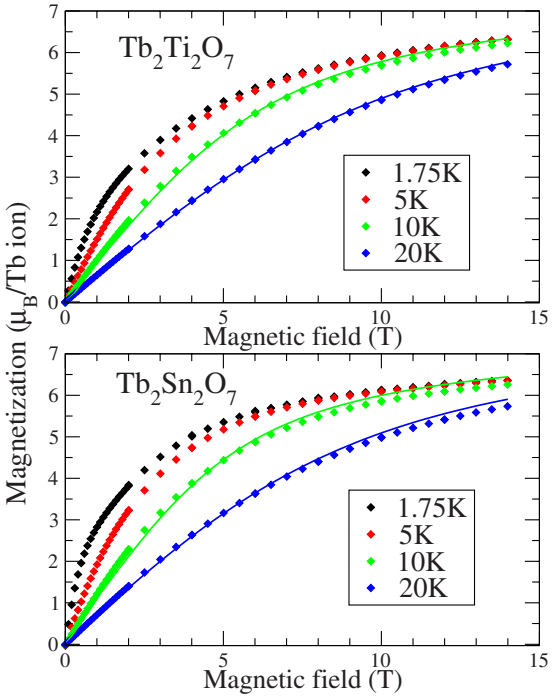

FIG. 13. (Color online) Isothermal magnetization in $Tb_2Ti_2O_7$ and $Tb_2Sn_2O_7$. The lines are self-consistently calculated curves at 10 and 20 K using the respective CF parameter sets in Eqs. (7) and (10) and an antiferromagnetic exchange constant $\lambda=-0.25\ \mathrm{T}/\mu_B$ for $Tb_2Ti_2O_7$ and $-0.20\ \mathrm{T}/\mu_B$ for $Tb_2Sn_2O_7$.

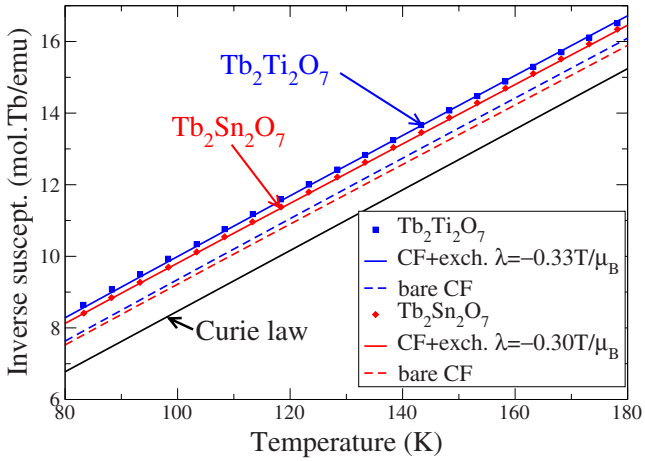

FIG. 14. (Color online) Inverse magnetic susceptibility in $Tb_2Ti_2O_7$ (blue symbols) and $Tb_2Sn_2O_7$ (red symbols) measured with a field of 0.005 T. The dashed lines are the crystal field only calculated curves using the respective parameter sets in Eqs. (7) and (10). The solid lines are the self-consistently calculated curves in the presence of crystal field and antiferromagnetic exchange, with $\lambda=-0.33\ \mathrm{T}/\mu_B$ for $Tb_2Ti_2O_7$ and $-0.30\ \mathrm{T}/\mu_B$ for $Tb_2Sn_2O_7$.

crystal field contribution $\theta_p^{CF}(T)$ on top of the usual exchange contribution θ_p^{ex}. This is clearly seen in Fig. 14, where the "bare CF" $1/\chi$ curves are drawn (dashed lines). As θ_p^{CF} shows a weak thermal variation, extraction of the effective θ_p value from extrapolation to zero of $1/\chi(T)$ is difficult.

For comparison with the experimental data, we used the B_n^m parameter sets derived from the inelastic neutron spectra to compute both $m(H)$ and $\chi(T)$ curves for a polycrystalline sample. We diagonalized the Hamiltonian,

$$\mathcal{H}=\mathcal{H}_{CF}+g_J\mu_B\mathbf{J}\cdot\mathbf{H}, \tag{13}$$

for a given orientation of $\mathbf{H}$. Then, the magnetization was calculated as $m(H,T)=g_J\mu_B\langle\mathbf{J}\cdot\mathbf{H}\rangle/H$, where $\langle\cdots\rangle$ stands for a thermal average over the crystal field levels and for an angular average over the applied field orientations. Interionic exchange and dipolar interaction were taken into account in the molecular field approximation via a microscopic constant λ. The total effective field experienced by a Tb^{3+} moment $\boldsymbol{\mu}$ is then $\mathbf{H}_{eff}=\mathbf{H}+\lambda\boldsymbol{\mu}$. The calculation is self-consistent, and convergence is reached only in the "paramagnetic phase" of the model, i.e., above a temperature T_t such that $k_BT_t\simeq\lambda\mu_0^2$. For both $m(H)$ and $\chi(T)$, we need an *antiferromagnetic* constant to reproduce the data. However, it was not possible to obtain a unique λ value adequate for both $m(H)$ and $\chi(T)$ data. In order to reproduce the high field magnetization curves at 10 and 20 K, we find $\lambda\simeq-0.25\ \mathrm{T}/\mu_B$ for $Tb_2Ti_2O_7$ and $-0.2\ \mathrm{T}/\mu_B$ for $Tb_2Sn_2O_7$ (see solid lines in Fig. 13). The magnitude of the molecular field at low temperature $H_{ex}=|\lambda|\mu_0$ is therefore about 1.2 T in both compounds. For the susceptibility data, we find $\lambda\simeq-0.33\ \mathrm{T}/\mu_B$ for the titanate and $-0.30\ \mathrm{T}/\mu_B$ for the stannate (see solid lines in Fig. 14). So, from both low field and high field data, the strength of the exchange is found smaller in the latter compound. For both compounds, $T_t\simeq5$ K, so the self-consistent calculation does not converge below about 8 K.

If the exchange and/or dipole interaction is written in terms of the total angular momentum $\mathbf{J}$ and of an effective integral $\mathcal{J}$ with the z nearest neighbor Tb^{3+} ions ($z=6$), then, in the mean field approximation, $\mathcal{J}$ and the high temperature paramagnetic Curie temperature θ_p^{ex} write

$$\mathcal{J}=\frac{1}{z}g_J^2\mu_B^2\lambda \text{ and } \theta_p^{ex}=\lambda\frac{g_J^2J(J+1)\mu_B^2}{3k_B}. \tag{14}$$

As our simple single-ion molecular field model cannot take into account the correlations that develop among the Tb moments at low temperature, we think that the λ values obtained from the high temperature susceptibility data are more reliable to obtain an estimate of the exchange integral. The ground state magnetic moment μ_0 and the parameters describing the exchange (high temperature values) in both compounds are gathered in Table II.

VI. LOW TEMPERATURE ANISOTROPIC MAGNETIC PROPERTIES OF Tb^{3+}

The Tb^{3+} ion has an even number (8) of $4f$ electrons and is therefore a non-Kramers ion, where the crystal field can completely lift the degeneracy of the $J=6$ spin-orbit multiplet. This results in singlet CF states or, as in the present case of high local symmetry, in both singlets and doublets. The doublets are characterized by the fact that they are anisotropic, i.e., an external magnetic field or an exchange and/or dipole field induces a moment which is not along the field, except when the latter is parallel to the [111] symmetry axis

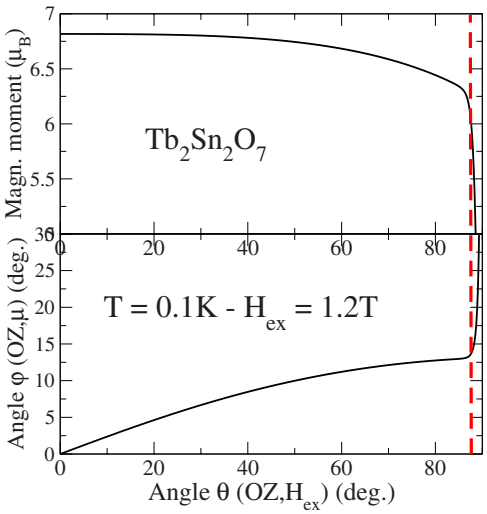

FIG. 15. (Color online) $Tb_2Sn_2O_7$: variation of the modulus μ and orientation φ of the magnetic moment induced by an exchange and/or magnetic field $\mathbf{H}_{ex}$=1.2 T, at 0.1 K, as a function of the angle θ of the field with Oz, where Oz is a [111] axis. The red dashed line is at θ=87.8° and could correspond to the actual situation in $Tb_2Sn_2O_7$.

or perpendicular to it. With a very small field, the doublets are extremely anisotropic, i.e., the moment is along [111] whatever the field direction. For a finite field value, the CF states are mixed and the induced magnetic moment $\boldsymbol{\mu}$ has components both along and perpendicular to [111].

Using the set of CF parameters in Eq. (10) appropriate for $Tb_2Sn_2O_7$, we have computed the modulus and orientation φ of the Tb^{3+} moment as the exchange field rotates from θ=0 to 90° (see Fig. 15) with respect to a given [111] axis Oz. For this purpose, we diagonalized Hamiltonian (13), where $\mathbf{H}$ is now an exchange field ($\mathbf{H}=\mathbf{H}_{ex}$), and we computed the magnetic moment $\boldsymbol{\mu}=-g_J\mu_B\langle\mathbf{J}\rangle$, where $\langle\cdots\rangle$ now stands for a thermal average only, as a function of the orientation θ of $\mathbf{H}_{ex}$.

We chose the value H_{ex}=1.2 T as derived above and a temperature T=0.1 K, well inside the LRO phase. As the field rotates, the moment remains close to Oz, with a quasi-saturated value of 13° as θ approaches 90°. Only when H_{ex} is very close to perpendicular to Oz (within a few degrees) does the moment start to abruptly reorient. Its modulus shows the same kind of behavior: it decreases very slowly from a value 6.8 μ_B for θ=0 and abruptly drops when the field is very close to perpendicular to Oz. Interestingly, for H=1.2 T, when θ=87.8°, one finds φ=14° and μ=5.9 μ_B (see the dashed line in Fig. 15), which are exactly the experimental values found in the LRO phase of $Tb_2Sn_2O_7$.[18] Whether this is a mere coincidence or not could be checked by carefully calculating the total field (exchange, dipolar, and possibly Dzyaloshinskii-Moriya) in the ordered spin ice phase of the latter compound. If one assumes, however, that, for symmetry reasons, the exchange and/or dipole field is along the ferromagnetic component of the moment, i.e., along a [001] direction, then θ=54.7° and one finds φ=10° and μ=6.7μ_B, which are not so far from the experimental data in view of the uncertainties inherent to the set of CF parameter values.[37]

In $Tb_2Ti_2O_7$, the same behavior is obtained, with, however, a lower value of 5.7μ_B of the maximum moment when θ=0.

VII. DISCUSSION

We successively discuss the CF parameters with regard to the crystal structure, the exchange constant deduced from the Curie-Weiss behavior, and the low energy excitation.

A. Crystal field parameters and crystal structure

The CF excitations in $Tb_2Ti_2O_7$ and $Tb_2Sn_2O_7$ show strong differences in their intensities, whereas their energies remain similar in the two compounds. Analyzing these excitations with the CF Hamiltonian shows that while the energy levels of the CF states remain similar, the dominant wave functions describing the ground state and first excited doublets are exchanged in the two compounds. This comes from a change in sign of the CF coefficient B_6^0. Such a change should come either from the substitution of the Ti^{4+} ion ($3d$) by Sn^{4+} (sp) or from small changes in the oxygen environment of a Tb^{3+} ion.

The crystal structure[27,28] is controlled by only two parameters, the lattice constant of the cubic cell a and the oxygen parameter u. The lattice constant at ambient temperature and pressure increases by 2.7% when going from $Tb_2Ti_2O_7$ [a =10.149(1) Å] to $Tb_2Sn_2O_7$ [a=10.426(1) Å]. The u parameter varies from 0.328(2) (Ti) to 0.336(2) (Sn).

In the cubic unit cell with space group $Fd\bar{3}m$, a given Tb^{3+} ion, corresponding to the 16d site (1/2,1/2,1/2) is surrounded by six oxygen O1 (48f sites) with position (3/8,3/8,1−u) and equivalent positions and two oxygen O2 (8b sites) with fixed positions (3/8,3/8,3/8) and (5/8,5/8,5/8). The oxygen environment of Tb^{3+} thus corresponds to a puckered ring of six O1 ions with long Tb-O1 distances (2.52 Å in $Tb_2Sn_2O_7$) and a linear O2-Tb-O2 unit with short Tb-O2 distances (2.26 Å in $Tb_2Sn_2O_7$), normal to the average plane of the puckered ring. The increase of u when going from Ti to Sn decreases the trigonal distortion around the Tb^{3+} ion, namely, the compression along the local [111] axis, the nondistorted case u=3/8=0.375 corresponding to eight equal Tb-O distances.

According to Ref. 29, the B_6^0 coefficient is proportional to a sum over the charges q_j surrounding the Tb^{3+} ion, which have coordinates (R_j,θ_j,φ_j) in a frame with Oz=[111]:

$$B_6^0 \propto \sum_j q_j \frac{Z_6^0(\theta_j,\varphi_j)}{R_j^7}, \tag{15}$$

where Z_6^0 is the tesseral harmonics proportional to

$$Z_6^0(\theta,\varphi) \propto 231\cos^6\theta - 315\cos^4\theta + 105\cos^2\theta - 5. \tag{16}$$

By considering only a sum over the eight oxygen neighbors, we calculated B_6^0 in the two compounds according to Eq. (15). We find that one cannot explain in such a way the change of sign of B_6^0 between the two compounds. The calculated parameters differ only by 13%. It means that either the point charge model is not suitable here or it should be extended to further neighbors.

B. Exchange interaction and Curie-Weiss constant

The determination of the exchange constant in these two compounds is important as input for the models trying to explain why the stannate shows magnetic LRO and the titanate does not. This estimation is usually achieved through measurement of the paramagnetic Curie temperature θ_p. In this work, we used the microscopic molecular field constant λ extracted from the high temperature susceptibility to obtain the θ_p^{ex} value, i.e., the contribution from exchange and/or dipolar interactions alone. It is found to be −7.0(3) K in $Tb_2Ti_2O_7$ and −6.3(3) K in $Tb_2Sn_2O_7$. The usual method to obtain θ_p is to measure the inverse susceptibility and to fit its linear thermal variation (if any) to the Curie-Weiss law. However, as it was already noticed in Ref. 14 and as it is clear from Fig. 14, in the Tb pyrochlores, with a very large overall CF splitting (about 800 K for $Tb_2Ti_2O_7$ and 600 K for $Tb_2Sn_2O_7$), the bare Curie-Weiss law does not hold in the usual temperature range of measurements (below 300–400 K). A first approximation is to write θ_p as a sum of two contributions, one due to exchange and/or dipolar interactions, the other to the CF splitting: $\theta_p = \theta_p^{ex} + \theta_p^{CF}(T)$. The CF contribution is weakly temperature dependent and is always of AF type, i.e., it always enhances the inverse susceptibility with respect to the Curie law. In Ref. 14, θ_p was measured in the dilute system $(Tb_{0.02}Y_{0.98})Ti_2O_7$ and found to be $\simeq -6$ K. As the exchange contribution to θ_p is zero in the dilute compound, this value was considered to be θ_p^{CF} appropriate in $Tb_2Ti_2O_7$; since in the latter compound $\theta_p \simeq -19(1)$ K,[14] θ_p^{ex} was estimated at $\simeq -13$ K.

We used the set of B_{nm} parameters derived here to calculate the bare CF susceptibility (dashed lines in Fig. 14). In $Tb_2Ti_2O_7$, we estimate $\theta_p^{CF} \simeq -9(1)$ K in the temperature range 150–300 K; in $Tb_2Sn_2O_7$, we estimate it at the somewhat lower value −7(1) K. The total paramagnetic Curie temperature predicted in our model would then be $\simeq -16(2)$ and $\simeq -13(2)$ K, respectively, in the titanate and in the stannate, while the experimental values[14,32,33] are −19(1) and −11(1) K, respectively. Therefore, our model is in relatively good agreement with published θ_p values, although we think one cannot obtained reliable values (within a few Kelvin) by the extrapolation method.

Our estimation of θ_p^{ex} in $Tb_2Ti_2O_7$ is about twice smaller than in Ref. 14 (−13 K). The associated exchange constant ($\mathcal{J} = -0.083$ K) is also smaller than quoted in Refs. 5 and 25 ($\mathcal{J} = -0.167$ K). The near neighbor exchange constant J_{nn} defined in Refs. 7 and 34 is deduced[35] from $\mathcal{J}$ by the expression $J_{nn} = \frac{1}{3g_J^2}\mathcal{J}(\mu_0/\mu_B)^2$. So, we get J_{nn} values of −0.32 and −0.39 K for $Tb_2Ti_2O_7$ and $Tb_2Sn_2O_7$, respectively, namely, for $Tb_2Ti_2O_7$ a smaller value than that of −0.9 K given in Ref. 34 (assuming a $|\pm 4\rangle$ ground state and $\mathcal{J} = -0.167$ K). Taking dipolar constants D_{nn} of 0.8 and 1.0 K for $Tb_2Ti_2O_7$ and $Tb_2Sn_2O_7$, respectively (D_{nn} varies as μ_0^2/a^3, where a is the lattice constant[34]), one gets J_{nn}/D_{nn} ratios of −0.4 and −0.39, respectively, for the Ti and Sn compounds, which locate them at the same position in the spin ice region of the phase diagram.[7] We conclude that the qualitative differences in the magnetic ground states of the two compounds cannot be understood simply within the approach given above.

C. Low energy excitation

In both compounds, a quasielastic signal is expected from (i) the energy width of the ground state CF level of the Tb^{3+} ion, of the same order of magnitude as the intrinsic linewidth of the inelastic lines, and (ii) the cooperative fluctuations of the Tb^{3+} moments in a given tetrahedron, yielding the spin liquid behavior. As the moments slow down, the width of this signal should decrease with temperature, as observed[4] in $Tb_2Ti_2O_7$.

An inelastic line can emerge from the quasielastic signal if the spin fluctuations become sufficiently slow so that the internal field becomes "static" (at the time scale of the neutron probe) and splits the energy levels of the ground state. The calculated typical energy of this splitting is around 0.01–0.1 THz (depending on the orientation and magnitude of the exchange field). Moreover, in $Tb_2Sn_2O_7$ which undergoes a transition toward long range order, cooperative ferromagnetic fluctuations of the tetrahedra start to grow below about 1.3 K.[18]

In the ordered phase, in order to get the full expression of the dynamical susceptibility, the total Hamiltonian need be written as the sum of a single-ion part (including the CF and the exchange term in the molecular field approximation) and an interionic part consisting of the exchange terms corrected from the molecular field. This was done, for instance, in Ref. 36. One expects to find both dispersion curves (spin waves) and flat modes (CF levels). In first approximation, in ordered $Tb_2Sn_2O_7$, the lowest energy branch should show a quadratic dispersion (expected for ferromagnetic like order) with a gap corresponding to the anisotropy constant D_a (where $D_a S_z^2 \sim \delta$ so that $D_a \sim 0.03$ THz). Checking this behavior in $Tb_2Sn_2O_7$ would require measuring the low energy excitations with a better energy resolution, if possible in a single crystal, above and below the ordering temperature.

VIII. CONCLUSION

Comparative measurements of the crystal field excitations by inelastic neutron scattering in $Tb_2Ti_2O_7$ and $Tb_2Sn_2O_7$ show important differences between the two compounds. We found a CF parameter set which accounts well for the inelastic features in $Tb_2Sn_2O_7$. The main difference with respect to $Tb_2Ti_2O_7$ is a change of sign of the B_6^0 CF parameter. This change cannot be simply explained by point charge calculations involving only the local oxygen environment of the Tb^{3+} ion. In $Tb_2Ti_2O_7$, fits of the high temperature susceptibility taking into account the crystal field scheme yield exchange and CF contributions to the Curie-Weiss constant which differ from previous evaluation. In $Tb_2Sn_2O_7$, the dispersion of a weakly inelastic excitation is suggested, which could be a precursor effect to the long range order.

ACKNOWLEDGMENTS

We are very thankful to A. Forget and D. Colson for the sample preparation. I.M. also thanks C. Lacroix, B. Canals, L. Levy, and M. Gingras for many interesting discussions.

[1] S. Bramwell and M. J. P. Gingras, Science **294**, 149 (2001).
[2] J. S. Gardner, S. R. Dunsiger, B. D. Gaulin, M. J. P. Gingras, J. E. Greedan, R. F. Kiefl, M. D. Lumsden, W. A. MacFarlane, N. P. Raju, J. E. Sonier, I. Swainson, and Z. Tun, Phys. Rev. Lett. **82**, 1012 (1999).
[3] J. S. Gardner, B. D. Gaulin, A. J. Berlinsky, P. Waldron, S. R. Dunsiger, N. P. Raju, and J. E. Greedan, Phys. Rev. B **64**, 224416 (2001).
[4] Y. Yasui, M. Kanada, M. Ito, H. Harashina, M. Sato, H. Okumura, K. Kakurai, and H. Kadowaki, J. Phys. Soc. Jpn. **71**, 2 (2002).
[5] Y. J. Kao, M. Enjalran, A. Del Maestro, H. R. Molavian, and M. J. P. Gingras, Phys. Rev. B **68**, 172407 (2003).
[6] M. Enjalran and M. J. P. Gingras, Phys. Rev. B **70**, 174426 (2004).
[7] B. C. denHertog and M. J. P. Gingras, Phys. Rev. Lett. **84**, 3430 (2000).
[8] I. Mirebeau, I. N. Goncharenko, S. T. Bramwell, M. J. P. Gingras, and J. S. Gardner, Nature (London) **420**, 54 (2002).
[9] I. Mirebeau, I. N. Goncharenko, G. Dhalenne, and A. Revcolevschi, Phys. Rev. Lett. **93**, 187204 (2004).
[10] K. C. Rule, J. P. C. Ruff, B. D. Gaulin, S. R. Dunsiger, J. S. Gardner, J. P. Clancy, M. J. Lewis, H. A. Dabkowska, I. Mirebeau, P. Manuel, Y. Qiu, and J. R. D. Copley, Phys. Rev. Lett. **96**, 177201 (2006).
[11] G. Luo, S. T. Hess, and L. R. Corrucini, Phys. Lett. A **291**, 306 (2001).
[12] N. Hamaguchi, T. Matsushita, N. Wada, Y. Yasui, and M. Sato, Phys. Rev. B **69**, 132413 (2004).
[13] I. Mirebeau, A. Apetrei, I. Goncharenko, and R. Moessner, Physica B **385-386**, 307 (2006).
[14] M. J. P. Gingras, B. C. denHertog, M. Faucher, J. S. Gardner, S. R. Dunsiger, L. J. Chang, B. D. Gaulin, N. P. Raju, and J. E. Greedan, Phys. Rev. B **62**, 6496 (2000).
[15] R. Siddharthan, B. S. Shastry, A. P. Ramirez, A. Hayashi, R. J. Cava, and S. Rosenkranz, Phys. Rev. Lett. **83**, 1854 (1999).
[16] S. Rosenkranz, A. P. Ramirez, A. Hayashi, R. J. Cava, R. Siddharthan, and B. S. Shastry, J. Appl. Phys. **87**, 5914 (2000).
[17] Y. M. Jana and D. Ghosh, Phys. Rev. B **61**, 9657 (2000).
[18] I. Mirebeau, A. Apetrei, J. Rodriguez-Carvajal, P. Bonville, A. Forget, D. Colson, V. Glazkov, J. P. Sanchez, O. Isnard, and E. Suard, Phys. Rev. Lett. **94**, 246402 (2005).
[19] J. D. M. Champion, S. T. Bramwell, P. C. W. Holdsworth, and M. J. Harris, Europhys. Lett. **57**, 93 (2002).
[20] F. Bert, P. Mendels, A. Olariu, N. Blanchard, G. Collin, A. Amato, C. Baines, and A. D. Hillier, Phys. Rev. Lett. **97**, 117203 (2006).
[21] P. Dalmas de Réotier, A. Yaouanc, L. Keller, A. Cervellino, B. Roessli, C. Baines, A. Forget, C. Vaju, P. C. M. Gubbens, A. Amato, and P. J. C. King, Phys. Rev. Lett. **96**, 127202 (2006).
[22] I. V. Alexandrov, B. V. Lidskii, G. Mamsurova, K. S. Pigal'skii, K. K. Pukhov, N. G. Trusevich, and L. G. Shcherbakova, Sov. Phys. JETP **62**, 1287 (1985).
[23] S. H. Curnoe, Phys. Rev. B **75**, 212404 (2007).
[24] A. K. Hassan and L. Levy (unpublished).
[25] H. R. Molavian, M. J. P. Gingras, and B. Canals, Phys. Rev. Lett. **98**, 157204 (2007).
[26] K. W. H. Stevens, Proc. Phys. Soc., London, Sect. A **65**, 209 (1952).
[27] J. E. Greedan, J. Mater. Chem. **11**, 37 (2001).
[28] A. Apetrei, I. Mirebeau, I. Goncharenko, and W. Crichton, J. Phys.: Condens. Matter **19**, 376208 (2007).
[29] M. T. Hutchings, Solid State Phys. **16**, 227 (1964).
[30] A. Abragam and B. Bleaney, *Electron Paramagnetic Resonance of Transition Ions* (Clarendon, Oxford, 1969).
[31] B. Z. Malkin, A. R. Zakirov, M. N. Popova, S. A. Klimin, E. P. Chukalina, E. Antic-Fidancev, Ph. Goldner, P. Aschehoug, and G. Dhalenne, Phys. Rev. B **70**, 075112 (2004).
[32] V. Bondah-Jagalu and S. T. Bramwell, Can. J. Phys. **79**, 1381 (2001).
[33] K. Matsuhira, Y. Hinatsu, K. Tenya, H. Amitsuka, and T. Sakakibara, J. Phys. Soc. Jpn. **71**, 1576 (2002).
[34] M. J. P. Gingras and B. C. den Hertog, Can. J. Phys. **79**, 1339 (2001).
[35] M. J. P. Gingras (private communication).
[36] A. Castets, D. Gignoux, and B. Hennion, Phys. Rev. B **25**, 337 (1982).
[37] A recent analysis of the neutron diffraction patterns in the ordered phase of $Tb_2Sn_2O_7$ reveals the presence of a sizeable short range ordered (SRO) moment. An estimation of the full magnetic moment at 0.1 K yields 6.6 (1) μ_B/Tb, which is actually close to the calculated value in the range $0 < \theta < 70°$. Thus taking the SRO moment into account, it cannot be concluded about the orientation of the total field with respect to the [111] axis.